GSJ: Volume 12, Issue 4, April 2024, Online: ISSN 2523-9376
www.globalscientificjournal.com

A NOVEL CONCEPT: TOWARDS SOLVING THE STARSHOT NANOCRAFT PROPULSION PROBLEM

Job Abianab Agyakinla

KeyWords
Concentric diamond beam, exoplanet, intergalactic sails, nanocraft, beamlets, beam arm, clearing beam, ultra-high-power, far field, beam radius, ring radius.

ABSTRACT

This paper presents a concept on ultra-high-power scaling capable of producing adequate laser beam power as the wind for propelling nanocrafts for intergalactic sails. The Concentric Diamond Beam (CDB) concept was conceptualized and developed with focus on the power requirement of the maiden starshot nanocraft propulsion project. In its simplest form, the concept involves beamlet sources arranged in concentric circles with optimal fill factor to ensure constructive interference at the far field. The concept consists of 33 equations derived to predict real world values of concept parameters required for early stage engineering and programming. Among others, the method makes it possible to determine the optimal number of beam arms for each ring, the distance covered by the nano-spacecraft, the angles at which beams from each ring should be shot to converge and the minimum distance of the clearing beam from the nanocraft. The clearing beam precedes the pushing beam to sweep the pathway for smooth sail. With eight underpinning assumptions, the concept aims at developing a novel approach that can generate adequate wind of propulsion to push nanocrafts to Prima Centauri b and other exoplanets in nearby galaxies. The concept will also be useful as a design for the construction of ultra-high-power laser missile defense systems.

I. Background

The dream of sailing space with high-power laser propelled nanocrafts is age long with Robert Forwards paper - Round Trip Interstellar Travel Using Laser-Pushed Lightsail - marking a major milestone (feasibility study)[1]. According to Robert Fugate (2017) the current generation is prepared for the implementation phase with some outlined physical, logistical, engineering, and legal challenges yet to be addressed[2].

The most popular among the physical problems is the struggle to gather adequate wind of propulsion to sail, direct and stabilize nanocrafts engineered for interstellar navigations[3,4,5]. The roadmap is led by conceptual attempts of power scaling of laser beams to the order of 100 gigawatts. So far, Tandem pumping and beam combining have been the two methods developed by scientists over the years with the latter leading the discourse due to its outstanding advantages over the former[6,7,8,9,10, 11,12].

The arrival of Coherent and Incoherent beam combining techniques pushed the frontiers of practical laser power scaling to the current limit[13,14,15,16,17] - the order of 100kW - which is below the required threshold for effective propulsion of nanocrafts. In order to realize the goal of laser beam propulsion and to benefit other applicable disciplines, there must be the possibility of efficiently combining millions of beams to obtain a single high-power beam output without compromising beam quality and stability[17,18,19,20]. Thermal challenges, optical issues, nonlinear effects and pumping power challenges are the limiting factors to generating high power output especially for single mode fiber lasers[22,23,24,25,26]. The five-year target set by Breakthrough Initiatives in 2017 to complete the conceptualization phase[27] is yet to be met seven years down the line.

This concept draws on heavily reviewed literature, related physical and mathematical theories to develop a novel approach of generating adequate laser power to push the first ever nanocraft to an exoplanet in Proxima Centauri star system and to future galaxies. This will brighten the chances of the human race to investigate Proxima Centauri b (a likely habitable planet in the Proxima Centauri system)3 and will broaden the scope of space science going forward. The concept will find its usefulness in laser missile weaponry technology and in building anti-missile defense systems

II. The Concentric Diamond Beam Concept

The concentric diamond Beam (CDR) concept consists of an arrangement of a finite number of laser beam sources in concentric rings to constitute a diamond-like structure as shown in Figure 1. As the beam angles are increased slowly and continuously, beam arms are lifted gradually, and P_i (point of convergence of all beams) is observed as a point object moving vertically upward from point P_0 to point P_3 and beyond. In the special scenario depicted in Figure 1, the beams from one ring initially converged at P_1 and then simultaneously increased beam angles gradually and continuously until they reached point P_2 and finally to point P_3. Each ring consists of closely packed beams as discussed further in later part of this paper. There can be as many rings as possible depending on the power requirement of the task ahead. To visualize the CDR concept, imagine each point on the circumference of a circular disc as a source of laser beam positioned to converge at a common focus Pi, which is equidistant from all points on the circumference. For simplicity sake, if we further imagine just four points on the circumference contributing to the output beam such that the four points form the vertices of a square, then we will obtain a diamond-like structure like Figure 1.

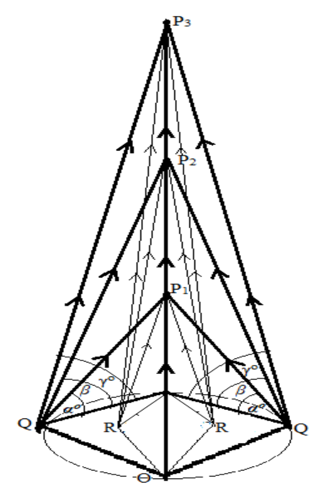

Figure 1. Beamlets from four vertices of a square touching the circumference of the first ring.

The Concentric Diamond Beam approach dwells on the following assumptions:

1. All input beams are homogenous with the same optical and geometric characteristics.
2. The input beams coherently combine at the far field.
3. At the point of convergence, the beams are coherent hence they will reinforce one another to scale up output beam power.
4. As the beam exit the earth's gravitational field, the workdone against gravity approaches zero and less beam power will be required for further propulsion.
5. As the nanocraft approaches the distant planet (eg. Prima Centauri b), gravitational pull by the planet further reduces workdone by the beam.
6. The minimum allowable increase in ring radius between two successive rings for maximum fill factor is D = 2r. Where D and r are beam diameter and radius, respectively.
7. Interstellar masses are asymmetric in shape to the clearing beam and will proceed in a random direction rather than the direction of sail when pushed by clearing beam.
8. The minimum effective value of beam angle occurs at $\alpha = 60^o$, at which Figure g becomes equilateral triangle as shown below.

GSJ: Volume 12, Issue 4, April 2024
ISSN 2320-9186

III. Inner Ring Arms and Outer Ring Arms

The diamond beam setup is made up of one inner ring of many closely packed beam arms surrounded by several outer rings. All the beam arms are oriented to focus at a point P_i, at a distance y_i, from the ground. Figure x shows the shooting of twelve beam arms of a single ring from the ground with O as the midpoint. All beam arms are equally spaced to ensure stability of the nanocraft motion.

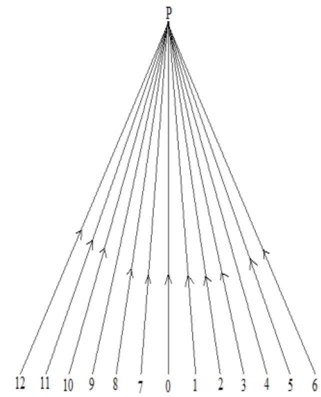

Figure x. Convergence of beams

Figure a. shows the arrangement of laser beam arms in the inner ring. If the radius of the ring formed by the densely packed laser beams is R and the radius of each beam in the ring is r, then from the figure b below,

$\sin \alpha^o = \frac{r}{r+R}$

$\alpha^o = \sin^{-1}(\frac{r}{r+R})$ --------------------------- (a)

From Figure a, the angle subtended by each circle is 2α at the center of the ring.

If there are *n* densely packed beam arms in the ring, then for the inner ring;

$n_o \times 2\alpha° = 360°$

$n_o = \frac{\pi}{\sin^{-1}(\frac{r}{r+R})}$ --------------------------- (1)

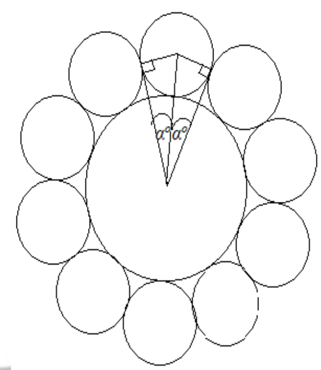

Figure a. Beam souces arranged in circular ring.

Equation (1) implies that, there can be finite number of laser beams in the inner ring. To get maximum value of n, $\sin^{-1}(\frac{r}{r+R})$ must be minimum which occurs at -1, but this can not be possible as it will yield n = -180 (negative number of beams). The possible range of values of $\sin^{-1}(\frac{r}{r+R})$ for which n is defined is {0 < $\sin^{-1}(\frac{r}{r+R})$ < 1}. Hence, for maximum n, the value of $\sin^{-1}(\frac{r}{r+R})$ must be as close as possible to zero but not zero.

Demonstrating the above with hypothetical values (i.e beam diameter of 0.1cm and ring diameter of R_0 = 100 cm);

$n_o = \frac{180}{\sin^{-1}(\frac{0.001}{0.001+1})}$

n_o = 314162 beam arms plus one middle beam.

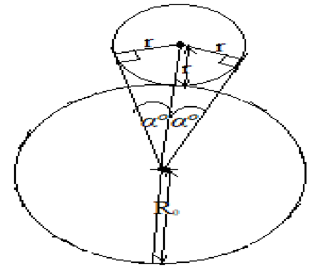

Figure b. Single beam held in position for simplicity of analysis

If each beam arm is to contribute input beamlet of power 100kW, then a combined beam power of around 31GW will be produced by the inner ring. This is less than the estimated 50 GW threshold for the nanocraft propulsion mission. However, an addition of the first order ring will increase the output power to a value within the estimated range (50 GW – 100 GW) for nanocraft propulsion. If we were to maintain r at 0.1cm and reduce R_0 to as low as 5cm, then $n_o = \frac{180}{\sin^{-1}(\frac{0.001}{0.001+0.05})}$

n_o = 160 beam arms plus one middle beam.

IV. Inner Ring Arms and Outer Ring Arms

The CDR setup has an inner ring surrounded by outer beam rings in a concentric fashion. The inner ring houses a single beam arm in its middle that fires directly at the target at 90° to the horizontal. The first order ring envelopes the inner ring and the second, third and subsequent high rings follow in ascending order.

The first order ring has an incremental increase in radius of ***Γ***. The new ring diameter becomes R_0 + ***Γ***. From Figure c, the minimum value of ***Γ*** is D = 2r. From equation (1);

$n_1 = \frac{\pi}{sin^{-1}(\frac{r}{r+R_0})}$ but $R_1 = R_0 + \boldsymbol{\Gamma}$

$n_1 = \frac{\pi}{sin^{-1}(\frac{r}{r+\Gamma+R_0})}$ The minimum allowable value of ***Γ*** will be Γ_0 = D = 2r

$n_1 = \frac{\pi}{sin^{-1}(\frac{r}{r+2r+R_0})}$

$n_1 = \frac{\pi}{sin^{-1}(\frac{r}{3r+R_0})}$ --------------------------- (2)

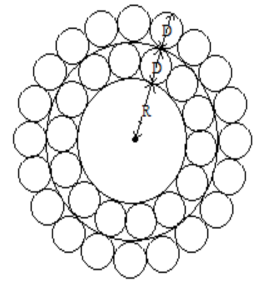

Figure c. First order ring

Comparing equation (1) and equation (2), it can be inferred that, for the same value of r and R, $n_1 < n_0$. For instance, subjecting equation (2) to the values in our earlier scenario (r = 0.1 cm and R = 5 cm) reveals that, $n_1 \approx n_0 + 6$.

The second order ring is the next ring of laser beam arms to the first order ring. Just as the first order ring, the ring radius increases by an incremental value of ***Γ***. The ring radius of the second order ring becomes $R_2 = R_1 + \boldsymbol{\Gamma} = R_o + 2\boldsymbol{\Gamma}$

Again, from equation (1),

$n_2 = \frac{\pi}{sin^{-1}(\frac{r}{r+R_2})}$ but $R_2 = R_0 + 2\boldsymbol{\Gamma}$

For minimum value of ***Γ***, ***Γ*** = D = 2r

$R_2 = R_o + 4r$

$n_2 = \frac{\pi}{sin^{-1}(\frac{r}{r+4r+R_0})}$

$n_2 = \frac{\pi}{sin^{-1}(\frac{r}{5r+R_0})}$ --------------------------- (3)

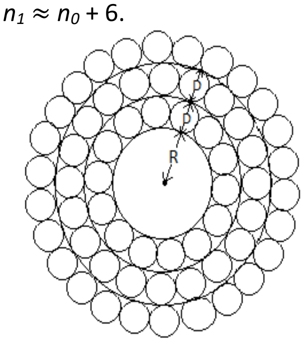

Figure e. Beams in the 2nd order ring.

Again, iterating with 0.1 cm$\leq R \leq 100\ cm$ and constant r = 0.1 cm, reveals that $n_1 \approx n_1 + 6$ and $n_2 \approx n_0 + 2(6)$

The third order ring comes after the second order ring and has an extension of ring radius by ***Γ***. This implies that, $R_3 = R_2 + \boldsymbol{\Gamma}$From equation (1),

$n_3 = \frac{\pi}{sin^{-1}(\frac{r}{r+R_3})}$ but ***Γ***= D = 2r

$n_3 = \frac{\pi}{sin^{-1}(\frac{r}{r+\Gamma+R_2})}$, but $R_2 = R_o + 2\boldsymbol{\Gamma}$

$n_3 = \frac{\pi}{sin^{-1}(\frac{r}{r+3\Gamma+R_0})}$

$n_3 = \frac{\pi}{sin^{-1}(\frac{r}{r+6r+R_0})}$

$n_3 = \frac{\pi}{sin^{-1}(\frac{r}{7r+R_0})}$ -------------------- (4)

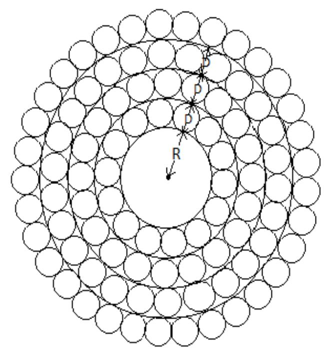

Figure f. Beams in the 3rd order ring.

We have shown from iteration with values of R between 0.1 cm and 100 cm that,

$n_o \approx n_0 + 0(6)$, $n_1 \approx n_0 + 1(6)$, $n_2 \approx n_0 + 2(6)$, $n_3 \approx n_0 + 3(6)$

Hence, $n_i \approx n_0 + i(6)$ -------------------- (5)

for i = 0, 1, 2, 3, ……………… N.

From iteration with the same values of R and r, we can generalize equation (1) as

$n_i = \frac{\pi}{sin^{-1}(\frac{r}{(2i+1)r+R_0})}$ -------------------- (6)

Also, we can show that,

$R_i = R_0 + i\boldsymbol{\Gamma}$ -------------------- (7)

for i = 0, 1, 2, 3, ……………… N

and for all values of R at a beam radius of 0.1 cm.

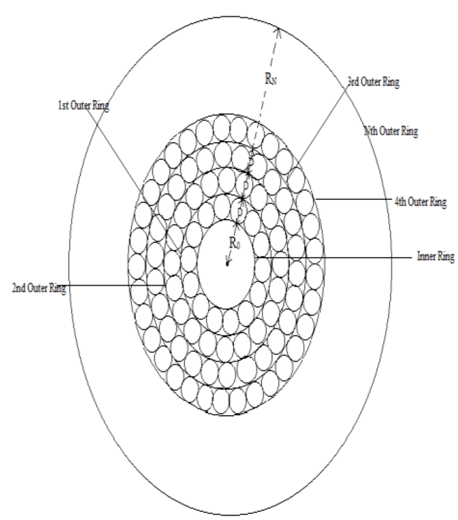

Figure g. Beams in the Nth ring.

V. Sail Displacement and Beam Displacement

For simplicity sake, we consider a single beam arm targeted at a fix point P in space as shown on Figure j. This can be extracted from Figure 1. Considering the cosine rule,

$y^2 = x^2 + z^2 - 2xz \cos \alpha$ ------------------------ (a)

but z can not be measured directly and so with sine rule, we attempt to eliminate it.

$$\frac{y}{\sin \alpha} = \frac{z}{\sin\theta}$$

$$z = \frac{\sin\theta}{\sin \alpha} y$$

Substituting this into equation (a),

$$y^2 = x^2 + \left(\frac{\sin\theta}{\sin \alpha} y\right)^2 - 2x\left(\frac{\sin\theta}{\sin \alpha} y\right) \cos \alpha$$

$$y^2 = x^2 + \frac{\sin^2\theta}{\sin^2\alpha} y^2 - 2xy\frac{\sin\theta \cos\alpha}{\sin\alpha}$$

rearranging the above equation,

$$\left[1 - \frac{\sin^2\theta}{\sin^2\alpha}\right] y^2 + \left[2x \frac{\sin\theta \cos\alpha}{\sin\alpha}\right] y - x^2 = 0$$

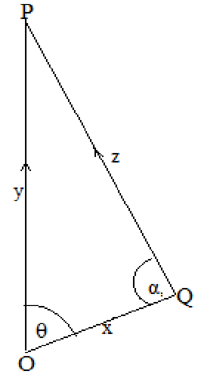

Figure j. Single beam focused at point P.

For simplicity sake, we consider a single beam arm targeted at a fix point P in space as shown on Figure j. This can be extracted from Figure 1. Considering the cosine rule,

$y^2 = x^2 + z^2 - 2xz \cos \alpha$ ------------------------ (a)

but z can not be measured directly and so with sine rule, we attempt to eliminate it.

$$\frac{y}{\sin \alpha} = \frac{z}{\sin\theta}$$

$$z = \frac{\sin\theta}{\sin \alpha} y$$

Substituting this into equation (a),

$$y^2 = x^2 + \left(\frac{\sin\theta}{\sin \alpha} y\right)^2 - 2x\left(\frac{\sin\theta}{\sin \alpha} y\right) \cos \alpha$$

$$y^2 = x^2 + \frac{\sin^2\theta}{\sin^2\alpha} y^2 - 2xy\frac{\sin\theta \cos\alpha}{\sin\alpha}$$

rearranging the above equation,

$$\left[1 - \frac{\sin^2\theta}{\sin^2\alpha}\right] y^2 + \left[2x \frac{\sin\theta \cos\alpha}{\sin\alpha}\right] y - x^2 = 0$$

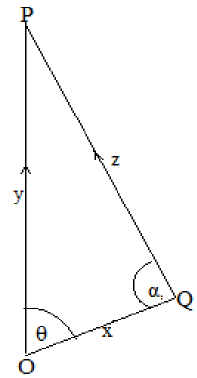

Figure j. Single beam focused at point P.

Comparing this to the general equation, $ay^2 + by + c = 0$ with the solution $y = \frac{-b \pm \sqrt{b^2 - 4ac}}{2a}$,

$a = 1 - \frac{\sin^2\theta}{\sin^2\alpha}$ $b = 2x \frac{\sin\theta \cos\alpha}{\sin\alpha}$ and $c = -x^2$

$$y = \frac{-2x\frac{\sin\theta \cos\alpha}{\sin\alpha} \pm \sqrt{\left(2x\frac{\sin\theta \cos\alpha}{\sin\alpha}\right)^2 - 4\left(1 - \frac{\sin^2\theta}{\sin^2\alpha}\right)(-x^2)}}{2\left(1 - \frac{\sin^2\theta}{\sin^2\alpha}\right)}$$

$$y = \frac{-2x\frac{\sin\theta \cos\alpha}{\sin\alpha} \pm 2x\sqrt{\left(\frac{\sin^2\theta \cos^2\alpha}{\sin^2\alpha}\right) + \left(1 - \frac{\sin^2\theta}{\sin^2\alpha}\right)}}{2\left(1 - \frac{\sin^2\theta}{\sin^2\alpha}\right)}$$

$$y = \frac{-2x\frac{\sin\theta \cos\alpha}{\sin\alpha} \pm 2x\sqrt{\left(\frac{\sin^2\theta \cos^2\alpha}{\sin^2\alpha}\right) + \left(1 - \frac{\sin^2\theta}{\sin^2\alpha}\right)}}{2\left(1 - \frac{\sin^2\theta}{\sin^2\alpha}\right)}$$

$$y = \frac{-2x\left[\frac{\sin\theta \cos\alpha}{\sin\alpha} \pm \sqrt{\left(\frac{\sin^2\theta \cos^2\alpha}{\sin^2\alpha}\right) + \left(1 - \frac{\sin^2\theta}{\sin^2\alpha}\right)}\right]}{2\left(1 - \frac{\sin^2\theta}{\sin^2\alpha}\right)}$$

$$= \frac{-[\frac{sin\theta\, cos\alpha}{sin\alpha} \pm \sqrt{\left(\frac{sin^2\theta\, cos^2\alpha}{sin^2\alpha}\right) + \left(1-\frac{sin^2\theta}{sin^2\alpha}\right)}]x}{(1-\frac{sin^2\theta}{sin^2\alpha})}$$

$$y = \frac{-[\frac{sin\theta\, cos\alpha}{sin\alpha} \pm \sqrt{\left(\frac{sin^2\theta\, cos^2\alpha}{sin^2\alpha}\right) + \left(1-\frac{sin^2\theta}{sin^2\alpha}\right)}]x}{(1-\frac{sin^2\theta}{sin^2\alpha})}$$

$$y = \frac{-[\frac{sin\theta\, cos\alpha}{sin\alpha} \pm \sqrt{1-sin^2\theta}]x}{(1-\frac{sin^2\theta}{sin^2\alpha})}$$

$$y = \frac{-[\frac{sin\theta\, cos\alpha}{sin\alpha} \pm \sqrt{cos^2\theta}]x}{(1-\frac{sin^2\theta}{sin^2\alpha})}$$

$$y = \frac{-[\frac{sin\theta\, cos\alpha}{sin\alpha} \pm \cos\theta]x}{(1-\frac{sin^2\theta}{sin^2\alpha})}$$

$$y = \frac{-[\frac{sin\theta\, cos\alpha \pm sin\alpha cos\theta}{sin\alpha}]x}{\frac{sin^2\alpha - sin^2\theta}{sin^2\alpha}}$$

$$y = \frac{\sin\theta \sin\alpha \cos\alpha \pm sin^2\alpha\, cos\theta}{sin^2\theta - sin^2\alpha} * x \qquad \text{------------------------ (8)}$$

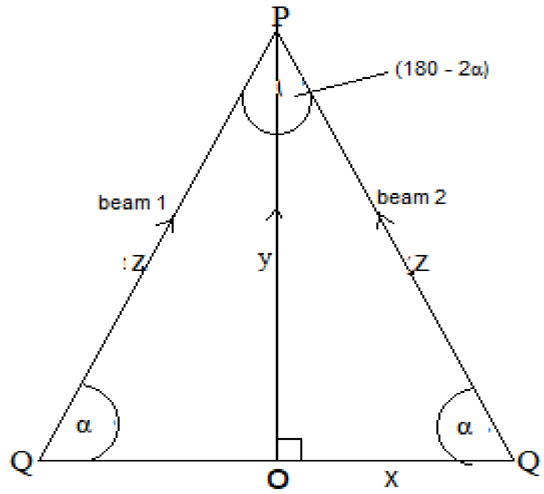

Figure k. Two beams from inner ring converging at P.

where y is the sail distance and α is the beam angle. If we maintain θ at 90°, then;

$$y = \frac{sin\alpha\, cos\alpha}{cos^2\alpha} * x$$

$$y = \frac{\sin\alpha}{\cos\alpha} * x$$

$$y = x \tan\alpha \qquad \text{------------------------ (9)}$$

From equation (9), y depends on x and tanα. But x is finite because we cannot have infinite ground space available. This implies that α lies between 0° and 90°. i.e $0° < \alpha < 90°$. As α approaches 90°, y approaches infinity which is desirable. With such a setup, the concentric beams can continue to converge/combine to push the target to the desirable destination.

From Figure j, if we fix θ at 90° and complete the other half of the triangle, we obtain Figure k. Applying Pythagoras theorem on this, $z^2 = y^2 + x^2$ and substituting y from equation (9),

$$z^2 = (x \tan\alpha)^2 + x^2$$

$$z = \sqrt{[x^2(\tan\alpha)^2 + 1)]}$$

$$z = x\sqrt{(\tan^2\alpha + 1)} \qquad \text{------------------------ (10)}$$

where z is the total distance travelled by the laser beam known as beam flight.

This equation is useful as it helps to determine how far the nanocraft has travelled based on the current beam angle and the distance of the beam source from the middle beam O. This is also useful in determining the beam velocity i.e Beam velocity $V_B = \frac{\Delta Z}{\Delta t}$.

$$V_B(t) = \frac{dZ}{dt} = \frac{d(x\sqrt{(\tan 2\alpha + 1)})}{dt} \qquad \text{------------------------ (11)}$$

and the beam acceleration will follow as $a_B(t) = \frac{dZ}{dt} = \frac{d(x\sqrt{(\tan 2\alpha + 1)})}{dt}$ ----------------- (12)

VI. Beam Shooting Angle

It is the angle at which all beam arms in a given ring must be shot to converge at a common focus, equidistant from all beams in the ring.

From Figure k and applying equation (8),

$$\alpha = \tan^{-1}(\frac{y}{x}) \qquad \text{------------------------(13)}$$

If we bring on first order ring to Figure k, we obtain Figure 3 as shown.

Applying equation (9), $y = x_1 \tan\beta$

$y = (x_o + \Gamma) \tan\beta$ since $x_1 = x_o + \Gamma$

but for maximum n, $\Gamma = D = 2r$

$y = (x_o + 2r) \tan\beta$

$\tan\beta = \frac{y}{(2r+x)}$

$$\beta = \tan^{-1}(\frac{y}{(2r+Xo)}) \qquad \text{------------------------(14)}$$

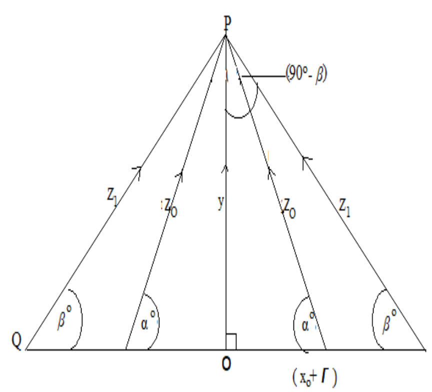

Figure 3. shooting angles of beams in the inner ring and 1st order ring.

For the first order ring to converge with the inner ring, ring arms must be oriented at β^o to the horizontal. If we add second order ring to Figure 3, we obtain Figure 4 as shown below.

It follows from equation (9) that, $y = (x_o + 2\boldsymbol{\Gamma})\tan\gamma^o$

Again for maximum n, $\boldsymbol{\Gamma} = D = 2r$

$y = (x_o + 4r)\tan\gamma^o$

$\tan\gamma^o = \left(\frac{y}{Xo + 4r}\right)$

$\gamma^o = \tan^{-1}\left(\frac{y}{Xo + 4r}\right)$ ------------------------ (15)

In a similar way, if we impose the third order ring on Figure 4, we obtain Figure 5 below. As more and more orders are added, Figure 5 begins to assume the shape of Figure x discussed earlier. From Figure 5. It follows from equation (9) that, $y = (x_o + 3\boldsymbol{\Gamma})\tan\eta^o$. Inserting $\boldsymbol{\Gamma} = D = 2r$ into the above,

$y = (x_o + 6r)\tan\eta^o$

$\tan\eta^o = \frac{y}{(Xo + 6r)}$

$\eta^o = \tan^{-1}\left(\frac{y}{(Xo + 6r)}\right)$ ----------------------- (16)

If we replace α, β, γ and η with α_o, α_1, α_2 and α_3 respectively. Comparing equations (13), (14), (15) and (16) we form the generalization that;

$\alpha_i = \tan^{-1}\left(\frac{y}{(Xo + 2ir)}\right)$ ---------------------- (17)

For i = 0, 1, 2, 3, …………………. N

Where α_i is the beam shooting angle for inner ring beams, first order beams, second order beams, third order beams and so on.

It follows from equation (9) that, $y = (x_o + 3\boldsymbol{\Gamma})\tan\eta^o$

Inserting $\boldsymbol{\Gamma} = D = 2r$ into the above,

$y = (x_o + 6r)\tan\eta^o$

$\tan\eta^o = \frac{y}{(Xo + 6r)}$

$\eta^o = \tan^{-1}\left(\frac{y}{(Xo + 6r)}\right)$ ------------------------(16)

If we consider α, β, γ and η as the angles subtended by the same beam arm at different positions, then we can replace α, β, γ and η with α_o, α_1, α_2 and α_3 respectively. Comparing equations (13), (14), (15) and (16) we can form a generalization that;

$\alpha_i = \tan^{-1}\left(\frac{y}{(Xo + 2ir)}\right)$ ------------------------(17)

For i = 0, 1, 2, 3, …………………. N

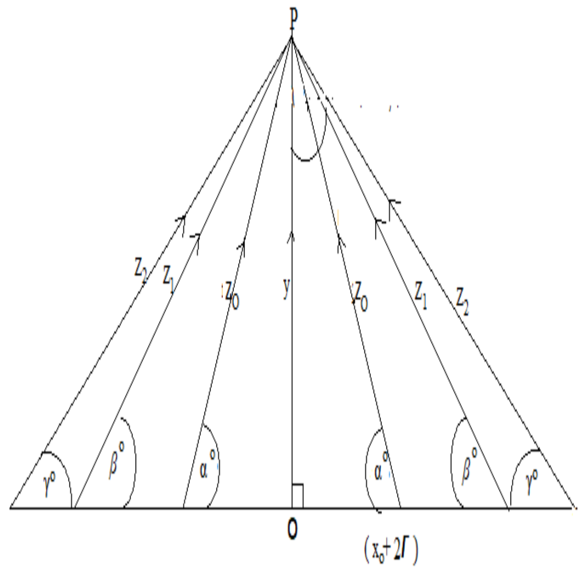

Figure 4. Shooting angles of beams in the inner ring, 1st and 2nd order rings.

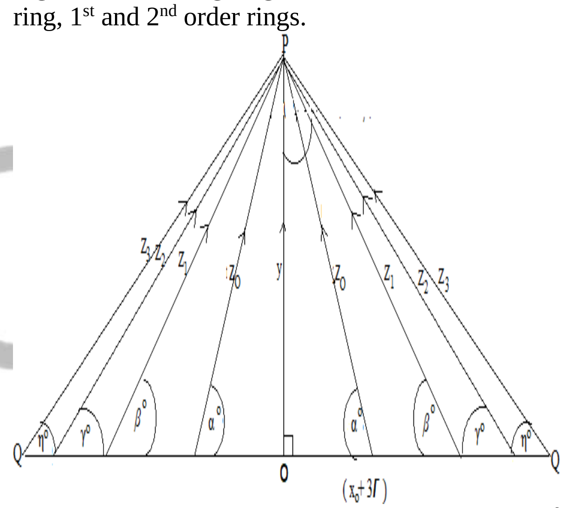

Figure 5. Shooting angles of the inner ring, 1st , 2nd, and 3rd order rings.

VII. Beam Velocity and Path Difference

From Figure k, $z_0^2 = y^2 + x_0^2$

But $y = x_o\tan\alpha_o$

$z_0^2 = (x_o\tan\alpha_o)^2 + x_0^2$

$z_0^2 = x_0^2\tan^2\alpha_0 + x_0^2$

$z_o = \sqrt{x_0^2\tan^2\alpha_0 + x_0^2}$ ------------------------ (18) or $z_o = x_0\sqrt{\tan^2\alpha_0 + 1}$

$z_o = x_0\sqrt{\sec^2\alpha_0}$, $z_o = \frac{x_0}{\cos\alpha_0}$ ------------------------ (19)

Also, from Figure 3

$z_1^2 = y^2 + x_1^2$, and $x_0 = x_0 + \boldsymbol{\Gamma} = x_0 + 2r$

Substituting this into the above,

$z_1^2 = y^2 + (x_o + 2r)^2$ but $y = x_o\tan\alpha_o$

$z_1^2 = x_0^2\tan^2\alpha_o + x_0^2 + 4x_or + 4r^2$

$z_1 = \sqrt{x_0^2\tan^2\alpha_0 + x_0^2 + 4x_0 r + 4r^2}$ ------------------------ (20)

Equation (20) gives the beam distance of the first order beams in terms of x_o, α_o and r. Also, from Figure 3,

$\sin\alpha_o = \frac{y}{z_0}$ ------------------------ (a)

$\sin\alpha_1 = \frac{y}{z_1}$ ------------------------ (b)

Dividing equation (b) by equation (a), $\frac{\sin\alpha 1}{\sin\alpha o} = \frac{z_1}{z_0}$

$z_1 = \frac{\sin\alpha 1}{\sin\alpha o} z_0$ ------------------------ (21), Taking the derivative of both sides of equation (21),

$\frac{dz_1}{dt} = \frac{\sin\alpha 1}{\sin\alpha o}\frac{dz_0}{dt}$ and $V_1(t) = \frac{\sin\alpha_1}{\sin\alpha_0} V_o(t)$ ------------------------ (22)

This implies that, for the beams in the two rings to arrive at point P at the same time, V_1 must be ($\frac{\sin\alpha 1}{\sin\alpha o}$) times faster than V_o, a condition difficult to achieve with lasers. Instead we focus on manipulating the time of trigger of beams for both rings. In the real world, we maintain the same velocity for all beams ($V_o = V_1 = V$) and then calculate the respective times of arrival for the beams in different rings as follows;

$t_o = \frac{zo}{v}$ and $t_1 = \frac{z1}{v}$

The trigger time difference is then calculated as $\Delta t = t_1 - t_o = \frac{z1-zo}{v}$

($z_o - z_1$) is the path difference between beams in the first order ring and those in the inner ring. In effect, the setup must be programmed in such a way as to allow the inner beams to be triggered ($\frac{z1-zo}{v}$) seconds earlier than beams in the first order ring. Since we can measure x_o, α_o and r from the setup, it is easier to predict z_1 and z_o from equations (18) and (20). Alternatively, from Figure 3,

$z_1^2 = y^2 + x_1^2$ but $y = x_1\tan\alpha_1$

$z_1^2 = x_1^2 \tan^2\alpha_1 + x_1^2$

$z_1 = \sqrt{[x_1^2 \sec^2\alpha_1]}$

$z_1 = \frac{x1}{cos\alpha 1}$ ------------------------ (23)

Also, from Figure 4,

$z_2^2 = y^2 + x_2^2$ but $y = x_2\tan\alpha_2$

$z_2^2 = x_2^2 \tan^2\alpha_2 + x_2^2$

$z_2^2 = x_2^2 \sec^2\alpha_2$

$z_2 = \frac{x2}{cos\alpha 2}$ ------------------------ (24)

Also from Figure 4,

$z_2^2 = y^2 + x_2^2$

$x_2 = x_o + 2\boldsymbol{\Gamma} = x_o + 4r$

Substituting this into the above,

$z_2^2 = y^2 + (x_o + 4r)^2$ but $y = x_o \tan\alpha_o$

$z_2^2 = x_o^2 \tan^2\alpha_o + x_o^2 + 8x_o r + 16r^2$

$z_2 = \sqrt{x_0^2\, tan^2\alpha_0 + x_0^2 + 8x_0 r + 16r^2}$ ------------------------ (25)

From Figure 5,

$z_3^2 = y^2 + x_3^2$ but $y = x_3\tan\alpha_3$

$z_3^2 = x_3^2 \tan^2\alpha_3 + x_3^2$

$z_3^2 = x_3^2 (\tan^2\alpha_3 + 1)$

$z_3 = \frac{x3}{cos\alpha 3}$ ------------------------ (26)

Alternatively, $z_3^2 = y^2 + x_3^2$

$x_3 = x_o + 3\boldsymbol{\Gamma} = x_o + 6r$

Substituting this into the above,

$z_3^2 = y^2 + (x_o + 6r)^2$ but $y = x_o \tan\alpha_o$

$z_3^2 = x_o^2 \tan^2\alpha_o + x_o^2 + 12x_o r + 36r^2$

$z_3 = \sqrt{x_0^2\, tan^2\alpha_0 + x_0^2 + 12x_0 r + 36r^2}$ ------------------------ (27)

Comparing equations (18), (20), (25) and (27), we can state that,

$z_i = \sqrt{x_0^2\,(tan^2\alpha_0 + 1) + 4ix_0 r + 4i^2r^2}$

$z_i = \sqrt{x_0^2\, sec^2\alpha_0 + 4ir(x_0 + ir)}$ ------------------------ (28)

where z_i is the beam displacement or beam path for the beams in rings i = 0, 1, 2, 3, ………… N.

Similarly, comparing equations (19), (23), (24) and (26), we can form the generalization that,

$z_i = \frac{xi}{cos\alpha_i}$ ------------------------ (29)

VIII. Vertical Motion (Sail Displacement)

If all the beam arms in each ring are programmed to raise gradually by increasing the beam angles, then point P will be viewed as an object moving vertically upwards. If we keep x constant and choose to vary y and α, we obtain Figure 6 as depicted below. From the diagram, the angle between the two beams converging at P_0 is $(180^0 – 2\alpha_0)$. At P_1, P_2 and P_3 the angles are $(180^0 – 2\alpha_1)$, $(180^0 – 2\alpha_2)$ and $(180^0 – 2\alpha_3)$ respectively.

In general, the angle subtended at the point of convergence by opposite beams in the i^{th} ring is $(180^0 – 2\alpha_i)$.

From our previous discussions, it can be shown that; $y_i = x \tan\alpha_i$ ------------------------ (30)

For a constant value of x

Equation (30) predicts the position of the beam, P_i from the ground for a given beam angle, α_i. This equation can also be useful in determining how far the nanocraft has travelled from earth.

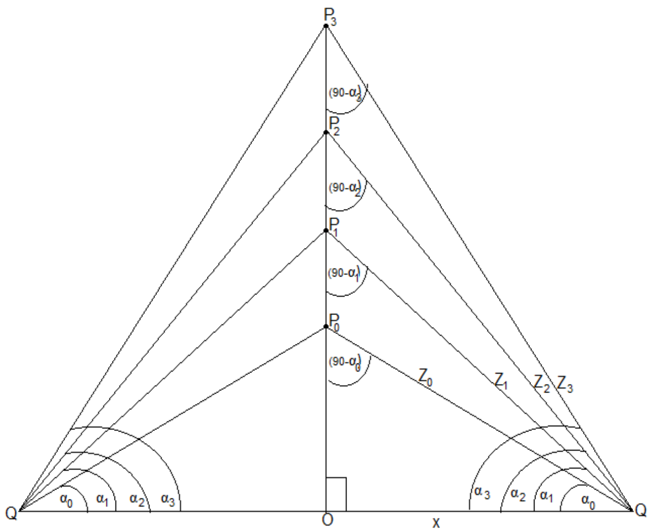

Figure 6. Vertical movement of two beams in the same ring form point P_1 to point P_2.

IX. **Path Clearing**

One of the challenges of the nanocraft propulsion concept is the possibility of continuous collision between the spacecraft and interstellar masses leading to unwanted retardation or total abortion of mission[37]. As long as the probability of occurrence of collision is greater than zero, it is necessary to address this challenge. From our analysis of vertical displacement, the point of convergence of beams in the ring can always be predicted. And so, in the last ring (clearing ring), all beams are programmed to converge at a certain distance ξ, ahead of the nanocraft. The clearing beam is expected to sweep the pathway of the spacecraft to reduce collisions. As shown in Figure 7, the minimum value of ξ will depend on the size of the spherical nanocraft.

Applying the Pythagoras theorem to ΔK_iOQ,

$(\xi + y_i)^2 = x^2 + S_i^2$ ------------------- (n)

Also, from sine rule with ΔK_iP_iQ,

$$\frac{\xi}{\sin(\sigma i - \alpha i)} = \frac{zi}{\sin(90 - \sigma)}$$

$$\xi = \frac{\sin(\sigma i - \alpha i)}{\cos \sigma i} z_i \quad \text{-------------------------- (m)}$$

Again using the sine rule with ΔK_iOQ,

$$\frac{\xi + yi}{\sin\sigma i} = \frac{x}{\sin(90 - \sigma i)}$$

$$\xi = \frac{\sin\sigma i}{\cos \sigma i} x - y_i \quad \text{--------------------------- (o)}$$

Comparing equation (m) and equation (o),

$$\frac{\sin(\sigma i - \alpha i)}{\cos\sigma i} z_i = \frac{\sin\sigma i}{\cos\sigma i} x - y_i$$

$$\left[\frac{\sin\sigma i \cos\alpha i)}{\cos\sigma i} - \frac{\sin\alpha i \cos\sigma i}{\cos\sigma i}\right] * z_i = \frac{\sin\sigma i}{\cos\sigma i} x - y_i$$

$$z_i \tan\sigma_i \cos\alpha_i - z_i \sin\alpha_i = x \tan\alpha_i - y_i$$

$$\tan\sigma_i = \frac{zi \sin\alpha i - yi}{zi \cos\alpha i - x}$$

$$\sigma_i = \tan^{-1}\left(\frac{zi \sin\alpha i - yi}{zi \cos\alpha i - x}\right) \quad \text{---------------------- (31)}$$

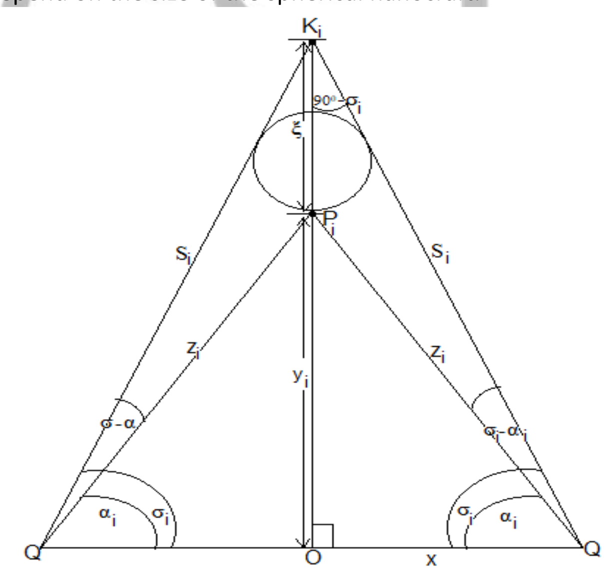

Figure 7. Path clearing beam ahead of the sail.

Since x is always known and y_i can be determined from $y_i = x \tan\alpha_i$, it is possible to predict the value of σ_i from equation (31). The value of z_i can be calculated from equation (28) or (29).

σ_i is known as the minimum allowable angle of the clearing beam. If the clearing beams are oriented at any angle less that σ_i, they will hit the nanocraft and the purpose for their creation will be defeated.

Substituting equation (31) into equation (o)

$$\xi = \frac{\sin\sigma i}{\cos \sigma i} x - y_i \quad = x \tan\sigma_i - y_i$$

$$\xi = x \tan\left[\tan^{-1}\left(\frac{zi \sin\alpha i - yi}{zi \cos\alpha i - x}\right)\right] - y_i$$

$$\xi = \frac{zi \sin\alpha i - yi}{zi \cos\alpha i - x} x - y_i \quad \text{---------------------------- (32)}$$

ξ is the minimum allowable distance between beams in the i^{th} ring and beams in the clearing ring.

Assumption:

Because interstellar masses are asymmetric in shape, the clearing beam will hit them off the pathway of the nanocraft as against sailing them ahead of the nanocraft perpetually.

Substituting equation (32) into equation (n),

$[(\frac{z_i \sin\alpha_i - y_i}{z_i \cos\alpha_i - x}x - y_i) + y_i]^2 = x^2 + S_i^2$

$(\frac{z_i \sin\alpha_i - y_i}{z_i \cos\alpha_i - x}x)^2 - x^2 = S_i^2$

$S_i = \sqrt{[(\frac{z_i \sin\alpha_i - y_i}{z_i \cos\alpha_i - x}x)^2 - x^2]}$ ---------------------------- (33)

X. Discusions

From the above, the paper showed that, laser beam power can be unlimitedly scaled by actively combining inputs from more beam arms. To achieve far field constructive interference of coherent beam inputs, the beams are packed to attain maximum fill factor[47]. This is desirable as more beamlets also imply higher combined beam output power. Inferring from equations (5) and (6), each ring can contain a finite number of beam arms for which coherent inference is expected to take place at the far field. The number of possible beam arms in a ring depends both on the beam radius and the ring radius. It was revealed that, for a given value of beam radius, the inverse sine of the ratio of beam radius to the sum of beam radius and ring radius must be as close as possible to zero, in order to achieve optimal number of beam arms. This implies that, more iterations will be required in real project implementation or simulation experiments to ascertain the best ring diameter that will match available ground space and beam radius. The optimal incremental increase in ring radius is predetermined by equation (7). This suggests that, more and more high-order rings can be added until the power requirement for the given project is met.

The results showed that, beams in the same ring can be programmed to converge at the same spot or in a small circular shape in which case we have spot convergence and circular convergence, respectively. This suggests two separate trials in determining the most stable module for the maiden project. In either case, the sail distance is predictable by equation (8) or equation (9). From equation (9), it can be predicted that, with the range of angles available to beamlets in the rings, the beams can travel close to infinity depending on beam angle orientation. Zero and ninety are forbidden values of beam angle and serve as an important note for engineers and programmers during prototype construction.

Beam flight or beam displacement can be predicted with equation (10) which is useful in determining whether beams from different rings positioned to converge at a point will arrive at the same time or not. Following the classical analysis (without interest in the relativistic relations) of equation (9), difference in time of arrival between beams from different rings exist. To circumvent this challenge, time differences should be considered during programming to ensure that, beams from higher order rings take off (by a calculated factor) before beams in lower rings. This arrangement ensures that all beams arrive at the same time to result in power gains from constructive interference at the far field. To achieve this, beams in the various rings must be shot at specific angles (beam shooting angles) as predicted by equation (17). It follows from simple iteration that, for the same displacement covered by the sail, beam angle decreases as we move outwards from inner ring towards the N^{th} ring. This is desirable as it implies that beams from different rings can never cross paths before reaching the point of interference.

Beam velocity is predictable with equation (22) and this can be an indicator of how fast or slow the nanocraft is travelling. This will serve as useful guide in determining how many years we need to arrive at Prima Centauri at a given rate of acceleration. The extremely high expected beam velocity reveals that, momentum will be high and impact of collisions with small interstellar masses may be significant. Especially if collisions are continuous. The Path Clearing beam sweeps the pathway off celestial debris to allow free travel of the nanocraft. Equation (31) predicts the minimum angle at which the path clearing beam can be shot without touching a spherical sail, while equation (32) predicts the minimum distance from the nanocraft at which path clearing beam can be targeted without touching the sail. Both equations forbid a path clearing beam angle of ninety degrees. Finally, equation (33) makes it possible to estimate the distance travelled by the path clearing beam. This distance may be used in varied applications including determining when to switch off path clearing beam to ensure energy efficiency.

XI. Conclusion

The CDB concept makes it possible to scale up laser beam power towards infinitesimally large magnitudes for intergalactic sails. This can be possible by completely avoiding passive components in the setup. Aside the ultrahigh power achievement, the concept allows for improved beam quality as constructive interference will take place at the far field. The combined power output from the arrangement depends on the power levels of the individual beamlets and especially the number of beam arms present. By extension ,the number of rings also affect the magnitude of output power. To ensure constructive interference at the far field ,lower order rings must be fully filled with beam arms before adding higher order rings .

Convergence of beams in a ring can be circular or spot and in both approaches the position of output beam depends on beam angles. Beamlets can be oriented to converge at positions close to infinity depending on project requirements and by adjusting beam angles .Beams from different rings will arrive at the same spot at different times and so trigger time for the various rings must be manipulated to achieve simultaneous arrival of all beams .With the CDR concept ,no two beamlets can cross paths before reaching the point of convergence .The concept makes it possible to predict the velocity of sail and by extension the duration of the entire journey at a given velocity and acceleration .The concept also allow for path clearing to avoid the consequence of continuous collision with celestial debris .

Overall ,the Starshot Nanocraft Propulsion mission should no longer be held backward by the physical limitation of low power scaling options. This paper presents an option to high-power scaling of laser input beams beyond the predicted range for propelling the maiden nanocraft sail. Besides, the CDR arrangement can sail continuously to distances close to infinity .

References

[1]. R. L. Forward, "Roundtrip interstellar travel using laser-pushed lightsails," Journal of Space-338 craft and Rockets 21(2), 187–194 (1984).

[2]. H. A. Atwater, A. R. Davoyan, O. Ilic, et al., "Materials challenges for the starshot lightsail," Nature Materials (2018).

[3]. Eliad Peretza, John C. Mathera, Christine Hamiltona et al., "Orbiting Laser Configuration and Sky Coverage: Coherent Reference for Breakthrough Starshot Ground-Based Laser Array"Journal of Astronomical Telescopes, Instruments, and Systems 8(1) (2022).

[4]. M. Noyes and M. Hart, "Analyzing the viability of satellite laser guide stars for breakthrough starshot," 6th International Conference on Adaptive Optics for Extremely Large Telescopes, AO4ELT (2019).

[5]. K. L. G. Parkin, "The breakthrough starshot system model," Acta Astronautica 152, 370–384 (2018).

[6]. Klenke, A.; Seise, E.; Limpert, J.; Tünnermann, A. Basic considerations on coherent combining of ultrashort laser pulses. Opt. Express (2011).

[7]. Uberna, R.; Bratcher, A.; Tiemann, B.G. Coherent Polarization Beam Combination. IEEE J. Quantum Electron (2010).

[8]. Zhu, J.; Zhou, P.; Ma, Y.; Xu, X.; Liu, Z. Power scaling analysis of tandem-pumped Yb-doped fiber lasers and amplifiers. Opt. Express (2011).

[9]. Chang, G.; Wei, Z. Ultrafast Fiber Lasers: An Expanding Versatile Toolbox. iScience (2020).

[10]. Fermann, M.E.; Hartl, I. Ultrafast Fiber Laser Technology. IEEE J. Sel. Top. Quantum Electron. (2009).

[11]. Design and Simulation of Next-Generation High-Power, High-Brightness Laser Diodes. IEEE J. Sel. Top. Quantum Electron (2009).

[12]. Zhu, J.; Zhou, P.; Ma, Y.; Xu, X.; Liu, Z. Power scaling analysis of tandem-pumped Yb doped fiber lasers and amplifiers. Opt. Express (2011).

[13]. Shi, C.; Su, R.T.; Zhang, H.W.; Yang, B.L.; Wang, X.L.; Zhou, P.; Xu, X.J.; Lu, Q.S. Experimental Study of Output Characteristics of Bi-Directional Pumping High Power Fiber Amplifier in Different Pumping Schemes. IEEE Photonics J. 9 (2017).

[14]. Lim, K.-J.; Kai-Wen Seah, S.; Yong'En Ye, J.; Lim, W.W.; Seah, C.-P.; Tan, Y.-B.; Tan, S.; Lim, H.; Sidharthan, R.; Prasadh, A.R.; et al. "High absorption large-mode area step-index fiber for tandem-pumped high-brightness high-power lasers". Photonics Res. (2020).

[15].

[16]. Fan, T.Y. Laser beam combining for high-power, high-radiance sources. IEEE J. Sel. Top. Quantum Electron. (2005).

[17]. Augst, S.J.; Ranka, J.K.; Fan, T.Y.; Sanchez, A. Beam combining of ytterbium fiber amplifiers. J. Opt. Soc. Am. B (2007).

[18]. Liu, Z.; Zhou, P.; Xu, X.; Wang, X.; Ma, Y. Coherent beam combining of high power fiber lasers: Progress and prospect. Sci. ChinaTechnol. Sci. (2013).

[19]. Liu, Z.; Ma, P.; Su, R.; Tao, R.; Ma, Y.; Wang, X.; Zhou, P. High-power coherent beam polarization combination of fiber lasers: Progress and prospect. J. Opt. Soc. Am. B (2017).

[20]. Bourdon, P.; Le Gouet, J.; Goular, D.; Lombard, L.; Durecu, A. Coherent Combining with Active Phase Control: A Practical Tool for Adaptive and Nonlinear Optics. In Proceedings of the 2017 Conference on Lasers and Electro-Optics Pacific Rim (CLEO-PR), Singapore (2017).

[21]. . Hanna, M.; Guichard, F.; Zaouter, Y.; Papadopoulos, D.N.; Druon, F.; Georges, P. Coherent combination of ultrafast fiber amplifiers. J. Phys. B At. Mol. Opt. Phys. (2016).

[22]. Sprangle, P.; Ting, A.; Penano, J.; Fischer, R.; Hafizi, B. Incoherent Combining and Atmospheric Propagation of High-Power Fiber Lasers for Directed-Energy Applications. IEEE J. Quantum Electron (2009).

[23]. Zervas, M.N. Power Scaling Limits in High Power Fiber Amplifiers due to Transverse Mode Instability, Thermal Lensing, and Fiber Mechanical Reliability. In Fiber Lasers XV: Technology and Systems; SPIE LASE 10512; SPIE Digital Library: San Francisco, CA, USA, (2018).

[24]. Zervas, M.N. Transverse mode instability, thermal lensing and power scaling in Yb3+ -doped high-power fiber amplifiers. Opt. Express (2019).

[25]. Zervas, M.N. Power Scaling Limits in High Power Fiber Amplifiers due to Transverse Mode Instability, Thermal Lensing, and Zervas, M.N. Transverse mode instability, thermal lensing and power scaling in Yb3+ -doped high-power fiber amplifiers. Opt. Express (2019).

[26]. Yang, B.; Wang, P.; Zhang, H.; Xi, X.; Shi, C.; Wang, X.; Xu, X. 6 kW single mode monolithic fiber laser enabled by effective mitigation of the transverse mode instability. Opt. Express (2021).

[27]. Jauregui, C.; Stihler, C.; Limpert, J. Transverse mode instability. Adv. Opt. Photonics (2020).

[28]. Li, Z.; Jing, F.; Li, C.; Liu, Y.; Luo, Q.; Lin, H.; Huang, Z.; Xu, S.; Yang, Z.; Wang, J. Impact of Stimulated Raman Scattering on the Transverse Mode Instability Threshold. IEEE Photonics J. (2018).

[29]. Robert Fugate, Breakthrough Starshot, Bidder's Briefing Phase 1 Sail RFP, May 23, 2018 Zoom Room.

[30]. Sarah Frazier, "An online article by ASA's Goddard Space Flight Center, Greenbelt, Md" (2019). https://www.nasa.gov/image-article/why-sun-wont-become-black-hole/.

[31]. Hossein F., Mikko N. and Regina G. "Towards Ultimate High-Power Scaling: Coherent Beam Combining of Fiber Lasers" Photonics (2021).

[32]. Zervas, M.N. Power Scalability in High Power Fibre Amplifiers. In Proceedings of the 2017 Conference on Lasers and ElectroOptics Europe & European Quantum Electronics Conference (CLEO/Europe-EQEC), Munich, Germany, 25–29 June (2017).

[33]. Codemard, C.A.; Sahu, J.K.; Nilsson, J. Tandem Cladding-Pumping for Control of Excess Gain in Ytterbium-Doped Fiber Amplifiers. IEEE J.

Quantum Electron. (2010).
[34]. Dai, J.; Li, F.; Liu, N.; Shen, C.; Zhang, L.; Li, H.; Li, Y.; Sun, S.; Li, Y.; Lv, J.; et al. Extraction of More than 10 kW from Yb-Doped Tandem-Pumping Aluminophosphosilicate Fiber. In Global Intelligent Industry Conference 2020; Wang, L., Ed.; SPIE: Bellingham, WA, USA, (2021).
[35]. Zhou, P.; Xiao, H.; Leng, J.; Xu, J.; Chen, Z.; Zhang, H.; Liu, Z. High-power fiber lasers based on tandem pumping. J. Opt. Soc. Am. B (2017).
[36]. Limpert, J.; Klenke, A.; Kienel, M.; Breitkopf, S.; Eidam, T.; Hadrich, S.; Jauregui, C.; Tunnermann, A. Performance Scaling of Ultrafast Laser Systems by Coherent Addition of Femtosecond Pulses. IEEE J. Sel. Top. Quantum Electron. (2014).
[37]. Klenke, A.; Muller, M.; Stark, H.; Kienel, M.; Jauregui, C.; Tunnermann, A.; Limpert, J. Coherent Beam Combination of Ultrafast Fiber Lasers. IEEE J. Sel. Top. Quantum Electron (2018) 36. Worden, W. Green, J. Schalkwyk, et al., "Progress on the starshot laser propulsion system," Applied Optics (2021).
[38]. Jauregui, C.; Limpert, J.; Tünnermann, A. High-power fibre lasers. Nat. Photonics (2013).
[39]. Liu, Z.; Jin, X.; Su, R.; Ma, P.; Zhou, P. Development status of high power fiber lasers and their coherent beam combination. Sci. China Inf. Sci. (2019).
[40]. Huang, L.; Yao, T.; Leng, J.; Guo, S.; Tao, R.; Zhou, P.; Cheng, X. Mode instability dynamics in high-power low-numerical-aperture step-index fiber amplifier. Appl. Opt. (2017)
[41]. Lin, H.; Xu, L.; Li, C.; Shu, Q.; Chu, Q.; Xie, L.; Guo, C.; Zhao, P.; Li, Z.; Wang, J.; et al. 10.6 kW high-brightness cascade-endpumped monolithic fiber lasers directly pumped by laser diodes in step-index large mode area double cladding fiber. Results Phys. (2019)
[42]. Wang, X.; Yan, P.; Wang, Z.; Huang, Y.; Tian, J.; Li, D.; Xiao, Q. The 5.4 kW Output Power of the Ytterbium-Doped Tandem Pumping Fiber Amplifier. In Proceedings of the Conference on Lasers and Electro Optics, San Jose, CA, USA, 13–18 May 2018;
[43]. Yang, B.; Wang, P.; Zhang, H.; Xi, X.; Shi, C.; Wang, X.; Xu, X. 6 kW single mode monolithic fiber laser enabled by effective mitigation of the transverse mode instability. Opt. Express (2021)
[44]. Klenke, A.; Hädrich, S.; Eidam, T.; Rothhardt, J.; Kienel, M.; Demmler, S.; Gottschall, T.; Limpert, J.; Tünnermann, A. 22 GW peak-power fiber chirped-pulse-amplification system. Opt. Lett. 2014.
[45]. Sprangle, P.; Hafizi, B.; Ting, A.; Fischer, R. High-power lasers for directed-energy applications. Appl. Opt. 2015
[46]. Ward, B.; Robin, C.; Dajani, I. Origin of thermal modal instabilities in large mode area fiber amplifiers. Opt. Express 2012
[47]. Brown, D.C.; Hoffman, H.J. Thermal, stress, and thermo-optic effects in high average power double-clad silica fiber lasers. IEEE J. Quantum Electron. 2001
[48]. Lockheed Martin Demonstrates 30 kW Weapons-Grade Fiber Laser. Available online: https://www.laserfocusworld.com/laserssources/article/16564243/lockheed-martin-demonstrates-30-kw-weaponsgrade-fiber-laser (accessed on 30 January 2014).
[49]. Mikhail A. Vorontsov and Svetlana L. Lachinova. Laser beam projection with adaptive array of fiber collimators. I. Basic considerations for analysis (2008).
[50]. Marc-André Lapointe, Stephane Chatigny, Michel Piché et al. Thermal effects in high power CW Fiber laser. Proceeding of SPIE (2009).
[51]. Fathi, H.; Närhi, M.; Gumenyuk, R. Towards Ultimate High-Power Scaling: Coherent Beam Combining of Fiber Lasers. Photonics (2021).
[52]. Andreas Tünnermann and Jens Limpert. Prospects and Challenges in High Power Fiber Laser Technology. OSA Technical Digest (CD) Optica Publishing Group (2011).
[53]. Smith, A.V.; Do, B.T.; Hadley, G.R.; Farrow, R.L. Optical Damage Limits to Pulse Energy from Fibers. IEEE J. Sel. Top. Quantum Electron. (2009).
[54]. Liu, A.; Chen, X.; Li, M.-J.; Wang, J.; Walton, D.T.; Zenteno, L.A. Suppressing nonlinear effects for power scaling of high power fiber lasers. Passiv Compon. Fiber-Based Devices IV (2007)
[55]. Li, T.; Ke, W.; Ma, Y.; Sun, Y.; Gao, Q. Suppression of stimulated Raman scattering in a high-power fiber amplifier by inserting long transmission fibers in a seed laser. J. Opt. Soc. Am. B (2019).
[56]. Jansen, F.; Nodop, D.; Jauregui, C.; Limpert, J.; Tünnermann, A. Modeling the inhibition of stimulated Raman scattering in passive and active fibers by lumped spectral filters in high power fiber laser systems. Opt. Express (2009).
[57]. Xu, H.; Jiang, M.; Shi, C.; Zhou, P.; Zhao, G.; Gu, X. Spectral shaping for suppressing stimulated-Raman-scattering in a fiber laser. Appl. Opt. (2017). Hadjifotiou, A.; Hill, G.A. Suppression of stimulated brillouin backscattering by psk modulation for high-power optical transmission. IEE Proc. J Optoelectron (1986).
[58]. Willems, F.W.; Muys, W.; Leong, J.S. Simultaneous suppression of stimulated Brillouin scattering and interferometric noise in externally modulated lightwave AM-SCM systems. IEEE Photonics Technol. Lett. (1994)
[59]. Zenteno, L.A.; Wang, J.; Walton, D.T.; Ruffin, B.A.; Li, M.J.; Gray, S.; Crowley, A.; Chen, X. Suppression of Raman gain in single-transverse-mode dual-hole-assisted fiber. Opt. Express (2005).
[60]. Yang, B.; Wang, P.; Zhang, H.; Xi, X.; Shi, C.; Wang, X.; Xu, X. 6 kW single mode monolithic fiber laser enabled by effective mitigation of the transverse mode instability. Opt. Express (2021)
[61]. Jauregui, C.; Stihler, C.; Limpert, J. Transverse mode instability. Adv. Opt. Photonics (2020) Li, Z.; Jing, F.; Li, C.; Liu, Y.; Luo, Q.; Lin, H.; Huang, Z.; Xu, S.; Yang, Z.; Wang, J. Impact of Stimulated Raman Scattering on the Transverse Mode Instability Threshold. IEEE Photonics J. (2018).
[62]. Mattia Caffa .Laser Diodes Power Scaling Techniques. Electronic Engineering (2020).
[63]. Christophe A. Codemard, Jayanta K. Sahu, and Johan Nilsson.Tandem cladding-pumping for control of excess gain in ytterbium-doped fiber amplifiers. IEEE Journal of Quantum Electronics (2011).
[64]. Christian Wirth, Oliver Schmidt, Andrea Kliner et al. High-power tandem pumped fiber amplifier with an output power of 2.9 kW.Optics Letters Vol. 36, Issue 16, pp. 3061-3063 (2011).

[65]. Wirth, C.; Schmidt, O.; Tsybin, I.; Schreiber, T.; Peschel, T.; Brückner, F.; Clausnitzer, T.; Limpert, J.; Eberhardt, R.; Tünnermann, A.; et al. 2 kW incoherent beam combining of four narrow-linewidth photonic crystal fiber amplifiers. Opt. Express (2009).
[66]. Lei, C.; Gu, Y.; Chen, Z.; Wang, Z.; Zhou, P.; Ma, Y.; Xiao, H.; Leng, J.; Wang, X.; Hou, J.; et al. Incoherent beam combining of fiber lasers by an all-fiber 7 × 1 signal combiner at a power level of 14 kW. Opt. Express (2018).
[67]. Wei-Zung Chang. Passive and Active Fiber Laser Array Beam Combining (2012). https://www.google.com/url?sa=t&source=web&rct=j&opi=89978449&url=https://deepblue.lib.umich.edu/bi.
[68]. Asher A. Friesem and Nir Davidson. Passive Beam Combining of Fiber Lasers.Frontiers in Optics (2008).
[69]. Qi Gao, Zhe Li, Wei Zhao, Gang Li al. Spectral beam combining of fiber lasers with 32 channels. Optical Fiber Technology (2023).
[70]. Ye Zheng, Zhanda Zhu, Xiaoxi Liu et al. High-power, high-beam-quality spectral beam combination of six narrow-linewidth fiber amplifiers with two transmission diffraction gratings. Appl Opt. (2019).
[71]. Jian Xu , Hongwei Gao , Yiting Xu. A hybrid incoherent sequence combining of pulsed lasers based on refraction-displacement-pulsed-combining and polarization beam combining. Optics Communications (2013).
[72]. Liu, Z.; Jin, X.; Su, R.; Ma, P.; Zhou, P. Development status of high power fiber lasers and their coherent beam combination. Sci. China Inf. Sci. 2019, 62, 41301. [CrossRef]
[73]. McClellan, M.; et al. 100-kW Coherently Combined Nd:YAG MOPA Laser Array. In Proceedings of the Frontiers in Optics (2009).
[74]. Goodno, G.D.; Shih, C.; Rothenberg, J.E. Perturbative analysis of coherent combining efficiency with mismatched lasers. Opt. Express (2010).
[75]. Leshchenko, V.E. Coherent combining efficiency in tiled and filled aperture approaches. Opt. Express (2015).
[76]. Ma, P.; Chang, H.; Ma, Y.; Su, R.; Qi, Y.; Wu, J.; Li, C.; Long, J.; Lai, W.; Chang, Q.; et al. 7.1 kW coherent beam combining system based on a seven-channel fiber amplifier array. Opt. Laser Technol (2021).
[77]. Müller, M.; Aleshire, C.; Klenke, A.; Haddad, E.; Légaré, F.; Tünnermann, A.; Limpert, J. 10.4 kW coherently combined ultrafast fiber laser. Opt. Lett. (2020).
[78]. Regelskis, K.; Gavrilinas, N.; Trusovas, R.; Raˇciukaitis, G. Coherent addition of orthogonally polarized fibre lasers with high combining efficiency. Lith. J. Phys. 2010
[79]. Fei Lu , Jianmin Li, Wei Zhang, Fei Tian et al. Far field output distribution features for spectral beam combining of diode laser array stack in an external cavity. Optik(2022).